Effect of the Mass Fraction of Ceramic Particles on the Porosity of Wear-Resistant Composites Fabricated by Combustion Synthesis

GUILIN SUN, DINGDONG FAN, and SUFEN TAO

Combustion synthesis was employed to fabricate a wear-resistant composite using reactions between Ti, Al, Fe_3O_4, B_4C, and CrO_3 powders on the steel plate. CaF_2 was used to improve the fluidity and decrease the melting temperature of Al_2O_3. A large number of holes were found in the top of the composite with different contents of ceramic particles. To elucidate the relationship between the mass fraction of ceramic particles and porosity, the adiabatic temperatures of different combustion systems were calculated. The porosity and size distribution of the holes of samples with different ceramic particle contents were studied, and the distributions and compositions of the ceramic particles were analyzed. The compositions surrounding and inside the holes were studied, and the hardness of the composite was also tested. The results show that the formation of holes is associated with the vaporization of Al and Cr. The porosity increases with an increase in the ceramic particle contents which is the combined effect of the decreasing adiabatic temperature, the increasing nucleation rate, the increasing ceramic particle sizes, the increasing viscosity of the metal, and the wetting angle between the liquid and solid phase, while the composition of ceramic particles has little effect. The hardness values of all composites exceed 60 HRC.

https://doi.org/10.1007/s11661-018-4839-1

I. INTRODUCTION

FABRICATING composites by incorporating ceramic reinforcements into a steel or iron matrix has attracted attention for their improved wear resistance, combined toughness and machinability properties related to the conventional steel or iron, and high hardness and good wear resistance related to the ceramic particles.[1–17] Among the various hard phases, TiC-TiB_2 has promising potential in engineering applications under extreme conditions owing to their excellent combination of mechanical and electrical properties, as well as their good corrosion and oxidation resistance at high temperature.[18] In addition, compared to conventional WC- and TiC-based cermets, TiC-TiB_2 composite-based cermets exhibit a higher hardness and chemical stability at high temperatures, and are regarded as a good alternative for wear-resistant applications. Therefore, TiC-TiB_2 is widely used as reinforcements in steel- or iron-matrix composites.[19]

Methods of fabricating TiC-TiB_2 reinforced steel- or iron-matrix composites include powder metallurgy,[1–3] conventional casting,[4–7] carbothermic reduction,[8–10] and self-propagating high-temperature synthesis (SHS).[11–15] SHS is the preferred technique owing to its high productivity, low cost, and high-purity products. In a previous study, most TiC or TiB_2 particles in reinforced steel- or iron-matrix composites reinforced the whole matrix, even if only a small area of the composite faced severe abrasion in practical applications, which is undoubtedly wasteful. Generally, Cr is used as an alloying element to improve the hardness of traditional wear-resistant steel, as well as ceramic particles. Therefore, in this work, reinforcements composed of a metal matrix (Fe and Cr) and ceramic particles (TiC and TiB_2) were combined with the steel matrix by combustion synthesis at a pressure of 1.5 MPa.

A higher mass fraction of TiC-TiB_2 in steel-matrix composites may not only result in higher hardness and better wear resistance, but also higher porosity, which was not considered in the previous study. Therefore, the aim of this study was to elucidate the relationship between the mass fraction of the ceramic particles and the porosity.

GUILIN SUN, DINGDONG FAN, and SUFEN TAO are with the School of Metallurgical Engineering, Anhui University of Technology, Ma'anshan, Anhui 243002, P.R. China and also with the Key Laboratory of Metallurgical Emission Reduction & Resources Recycling, Anhui University of Technology, Ministry of Education, Ma'anshan, Anhui 243002, P.R. China. Contact e-mail: ahuttsf@163.com

Manuscript submitted November 21, 2017.
Article published online July 26, 2018

Table I. Experimental Conditions

The Experimental Conditions				Raw Materials Quality (g)					
Pressure (MPa)	Mass Fraction of CaF_2 (Pct)	Mass Ratio of Fe/Cr	Mass Fraction of Ceramic Particles (Pct)	Al	CrO_3	Fe_3O_4	CaF_2	Ti	B_4C
1.50	2.00	4.00	5.00	26.16	18.27	52.48	1.01	1.80	0.70
1.50	2.00	4.00	10.00	24.77	17.31	49.71	0.96	3.60	1.40
1.50	2.00	4.00	15.00	23.40	16.35	46.95	0.90	5.40	2.10
1.50	2.00	4.00	20.00	22.02	15.38	44.19	0.85	7.20	2.80
1.50	2.00	4.00	25.00	20.65	14.42	41.43	0.80	9.00	3.50

II. EXPERIMENTAL

B_4C and Ti were used as the combustion system for the formation of ceramic TiC and TiB_2 particles. Fe_3O_4, CrO_3, and Al were used as the combustion system for the formation of Fe and Cr, based on the combustion synthesis and solidification theories. The Al_2O_3 produced by the reaction has a large density difference with the matrix, and will be removed by gravity as slag. To reduce its melting point and viscosity, and increase its fluidity, a certain amount of CaF_2 was added.

High-purity and fine Ti, Al, CaF_2, B_4C, and CrO_3 powders were used to fully prepare the combustion reaction. The powders' granularity was below 74 μm and their purity was over 99.99 pct. The Fe_3O_4 powder used in this experiment was obtained from the scales of the rolling process, which were ground into a powder with a granularity of 149 to 250 μm.

The combustion system was constructed based on the thermodynamic calculation and material design methods. It is assumed that, if the total amount of matrix-phase and ceramic particles is 50 g, CaF_2 constitutes 5 pct of the total slag, and the amount of each reactant is calculated as shown in Table I. The reactant was mixed and loaded in a cylindrical crucible with a diameter of 40 mm and height of 50 mm on the steel plate with a thickness of 16 mm, and placed into the reaction chamber, as shown in Figure 1. A tungsten coil was fixed above the upper surface of the powder. The reaction chamber was evacuated and subsequently filled with high-purity Ar gas to a pressure of 1.5 MPa. The top of the reactant compact was then ignited by passing an electric current of ~ 10 A through the tungsten coil for 2 seconds. Upon ignition, the reaction took place and the reactant rapidly transformed into the product, which was naturally cooled to 298 K in the reaction chamber and then extracted for measurement.

III. RESULTS AND DISCUSSION

Reaction temperature is a key factor in combustion synthesis, as it determines the physical states of reactants and products and has an important effect on the reaction mechanism and kinetics.[20–22] Assuming that the reaction system undergoes no heat exchange with the surrounding environment, the maximum reaction temperature under adiabatic conditions (Tad) can be calculated as follows:

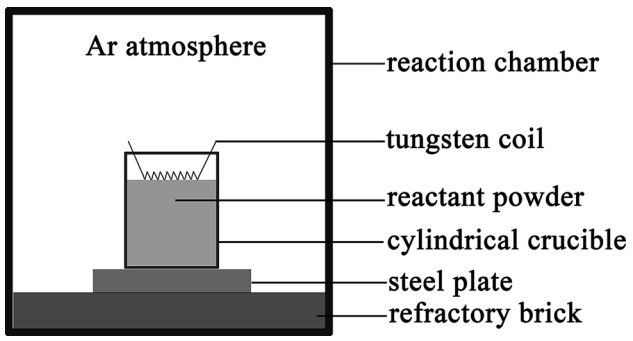

Fig. 1—An illustration for combustion synthesis experiment under an Ar atmosphere.

$$-\Delta H_{T_0} = \int_{T_0}^{T_{ad}} \sum n_i C_i \mathrm{d}T + \sum_{T_0}^{T_{ad}} n_i H_i, \qquad [1]$$

where T_0 is the initial reaction temperature, ΔH_{T_0} is the heat released by the combustion reaction, H_i is the enthalpy of the phase transformation of the product, and n_i and C_i are the stoichiometry and heat capacity of the product, respectively.

Changes in the mass fraction of ceramic particles affect the adiabatic combustion temperature of the system, which determines the floating time of the bubbles. Therefore, the adiabatic combustion temperatures of the binary Al-Fe_3O_4, Al-CrO_3, and Ti-B_4C systems were calculated using Eq. [1] and the relevant thermodynamic data.[23] The adiabatic combustion temperatures of the multicomponent Al-Fe_3O_4-CrO_3-B_4C-Ti system with a Fe/Cr mass ratio of 4 and ceramic particle mass fractions of 5, 10, 15, 20, and 25 pct were also calculated. The results of this are shown in Table II.

Table II shows that the T_{ad} is higher than the vapor point of Al (2767 K), and the melting points of Fe_3O_4 (1870 K), CrO_3 (470 K), and B_4C (2743 K). However, the T_{ad} of the Ti-B_4C binary system and the Al-Fe_3O_4-CrO_3-B_4C-Ti multicomponent is below the melting point of Ti (3290 K). Thus, the reaction occurs between the Al gas and Fe_3O_4 (CrO_3) liquid, and between the solid Ti particles and B_4C liquid, which will be self-sustained because the reaction temperature exceeds the

Table II. Adiabatic Temperatures of Different Combustion Systems

	Binary System			Ceramic Particle Mass Fraction of Multicomponent System Al-Fe_3O_4-CrO_3-B_4C-Ti (Pct)				
System	Al-Fe_3O_4	Al-CrO_3	Ti-B_4C	5	10	15	20	25
Adiabatic temperature (K)	3134	3967	2997	3144.77	3143.86	3143.59	3143.30	3142.96

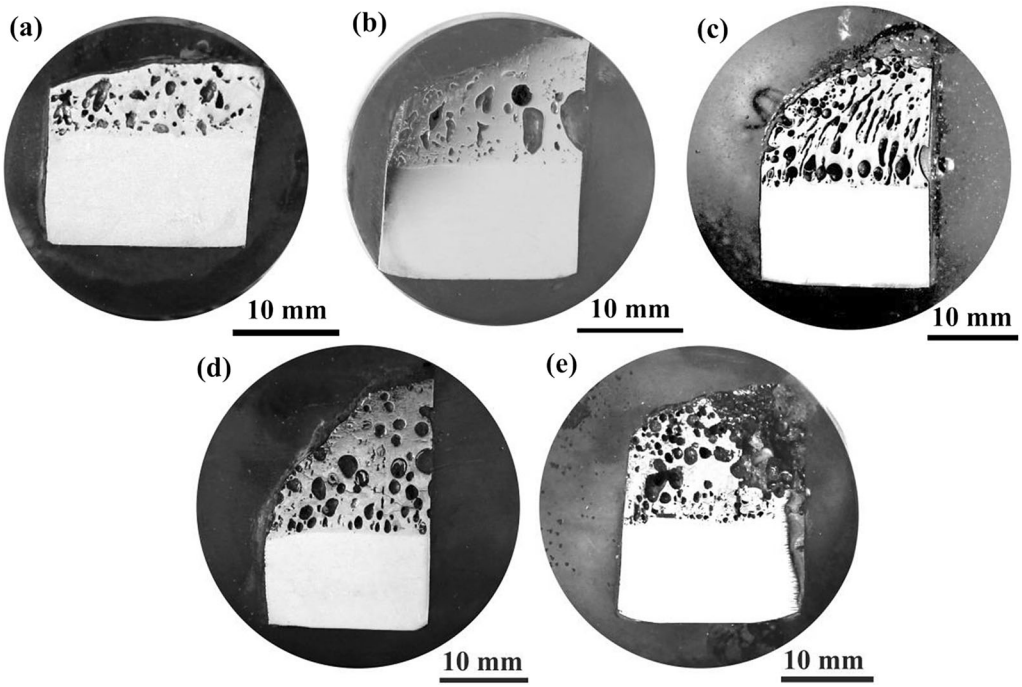

Fig. 2—Morphologies of products fabricated by combustion synthesis with different ceramic particle mass fractions: (*a*) 5 pct; (*b*) 10 pct; (*c*) 15 pct; (*d*) 20 pct; (*e*) 25 pct.

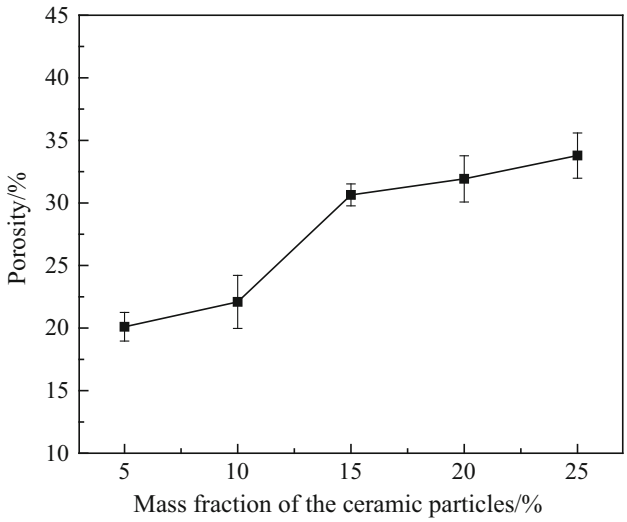

Fig. 3—Relationship between ceramic particle mass fraction and porosity.

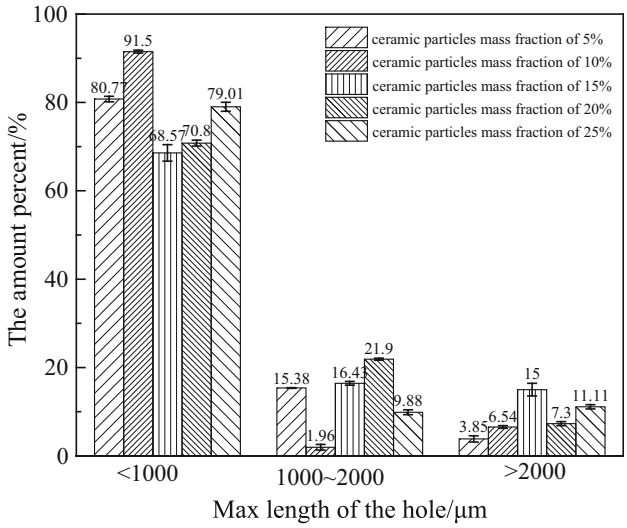

Fig. 4—Size distribution of the holes in the products with different ceramic particle masses.

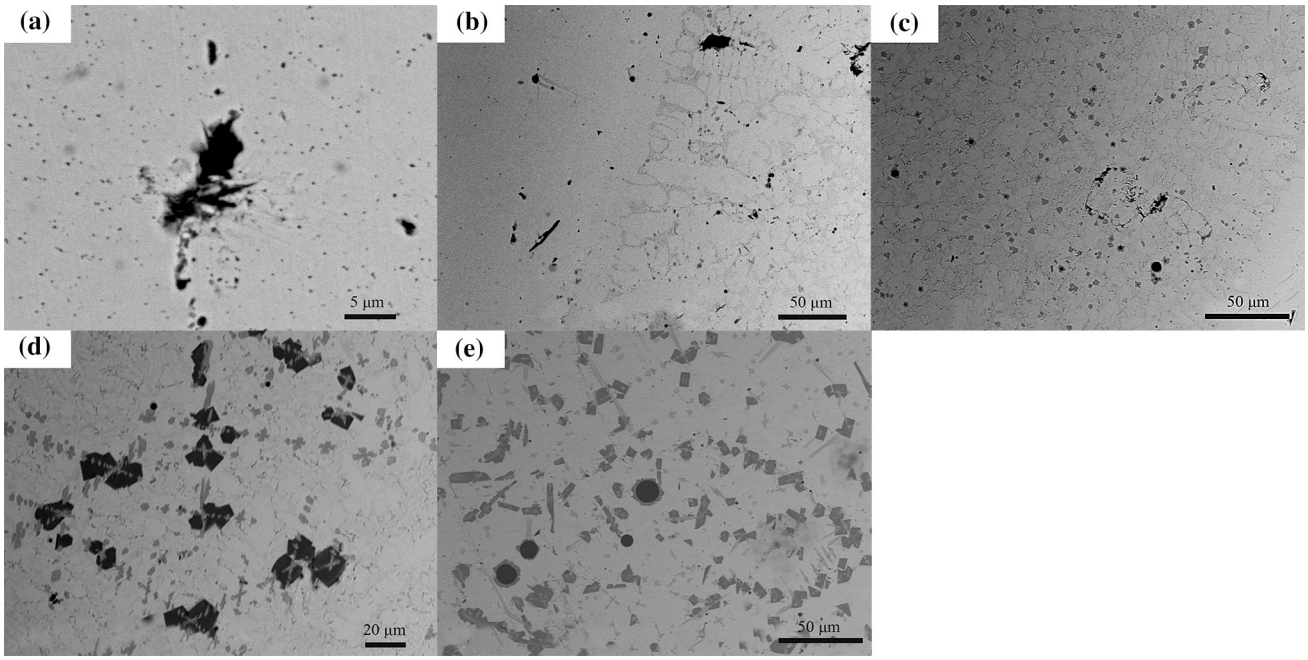

Fig. 5—SEM images for the distribution of ceramic particles with different mass fractions: (*a*) 5 pct; (*b*) 10 pct; (*c*) 15 pct; (*d*) 20 pct; (*e*) 25 pct.

melting point of at least one reactant.[24] Additionally, the mass fraction of the ceramic particles has little effect on the adiabatic temperature.

Figure 2 shows the morphologies of the products fabricated by combustion synthesis with different ceramic particle mass fractions, clearly showing the holes in the top (the product of the reaction). Therefore, to elucidate the relationship between the ceramic particle mass fraction and the porosity and size distribution of the holes, the number and sizes of holes were analyzed and the related statistics were plotted, as shown in Figures 3 and 4, respectively. The results show that the porosity increases with the ceramic particle mass fraction, but the ceramic particle mass fraction has little effect on the sizes of pores, most of which are smaller than 1000 μm. This may be related to the two phenomena described below. The adiabatic temperature of the system decreases as the ceramic particle contents increases, shortening the time required for the temperature of the reaction product to reach its freezing point, which decreases the probability of bubble flotation. However, ceramic particles can be the nuclei of bubbles, so the nucleation rate of bubbles increases as the content of ceramic particles increased.

The distribution of ceramic particles and their compositions were studied using scanning electron microscope (SEM) attached with energy disperse spectroscopy (EDS), and the results are shown in Figures 5 and 6. The ceramic particles are fine and dispersed when the mass fraction is below 10 pct. They grow within the local area as the mass fraction increases to 15 pct, and then expand throughout the composite as the mass fraction reaches and exceeds 20 pct. The EDS results show that the composition of the ceramic particles also changes with the mass fraction; when the mass fraction is below 15 pct, the composite contains Ti, B, and C, some of which nucleate on the Al_2O_3, but it contains either TiB_2 or TiC at mass fractions of 20 and 25 pct.

The composition of the ceramic particles has little effect on the porosity of the reaction product. The porosity increases with the ceramic particles mass fraction because of the growing ceramic particle sizes. The coarsening ceramic particles will not only damage the continuity of the base, but also effectively prevent the rise of bubbles.

To determine the formation mechanism of holes, SEM-EDS analysis was conducted on the area surrounding and inside the holes, and the results are shown

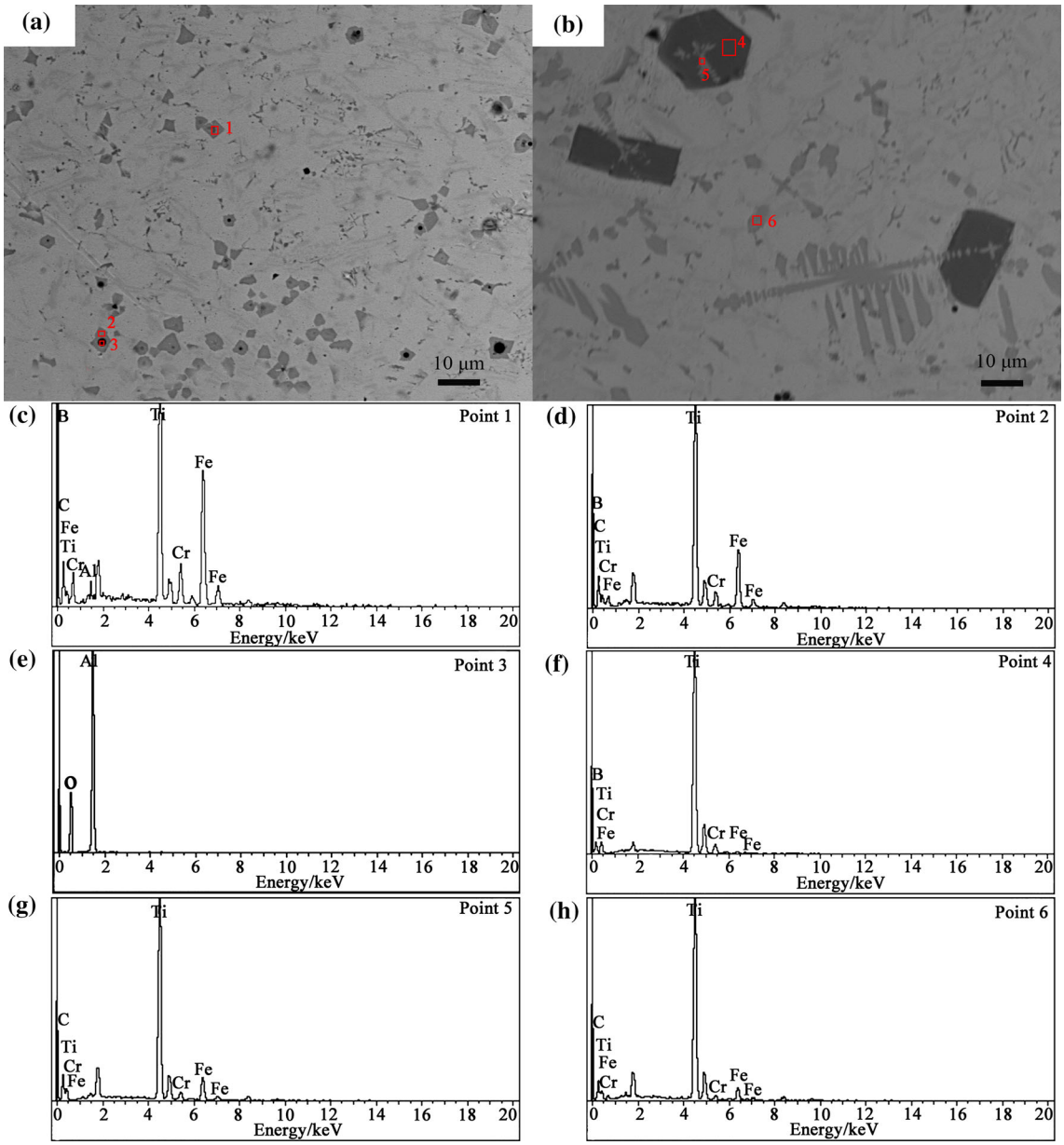

Fig. 6—SEM images and EDS results of the ceramic particles at different amounts: (*a*) 15 pct; (*b*) 20 pct; (*c*) through (*h*) EDS spectra for points 1 to 6 in (a) and (b).

in Figures 7 through 9. As shown in Figure 7, aluminum deposited on the pore surfaces of all the samples mentioned above, which is associated with the vaporization of the feedstock aluminum that generates gas bubbles, which can remain trapped inside the melt pool during solidification.[25]

The viscosity and wettability between the ceramic particles and the matrix had a great effect on the densification of the melt.[25–27] The temperature and viscosity of the melt pool decrease with increasing TiC and TiB_2 contents, thereby decreasing surface tension of the solid–liquid and melt flow, which in turn increases

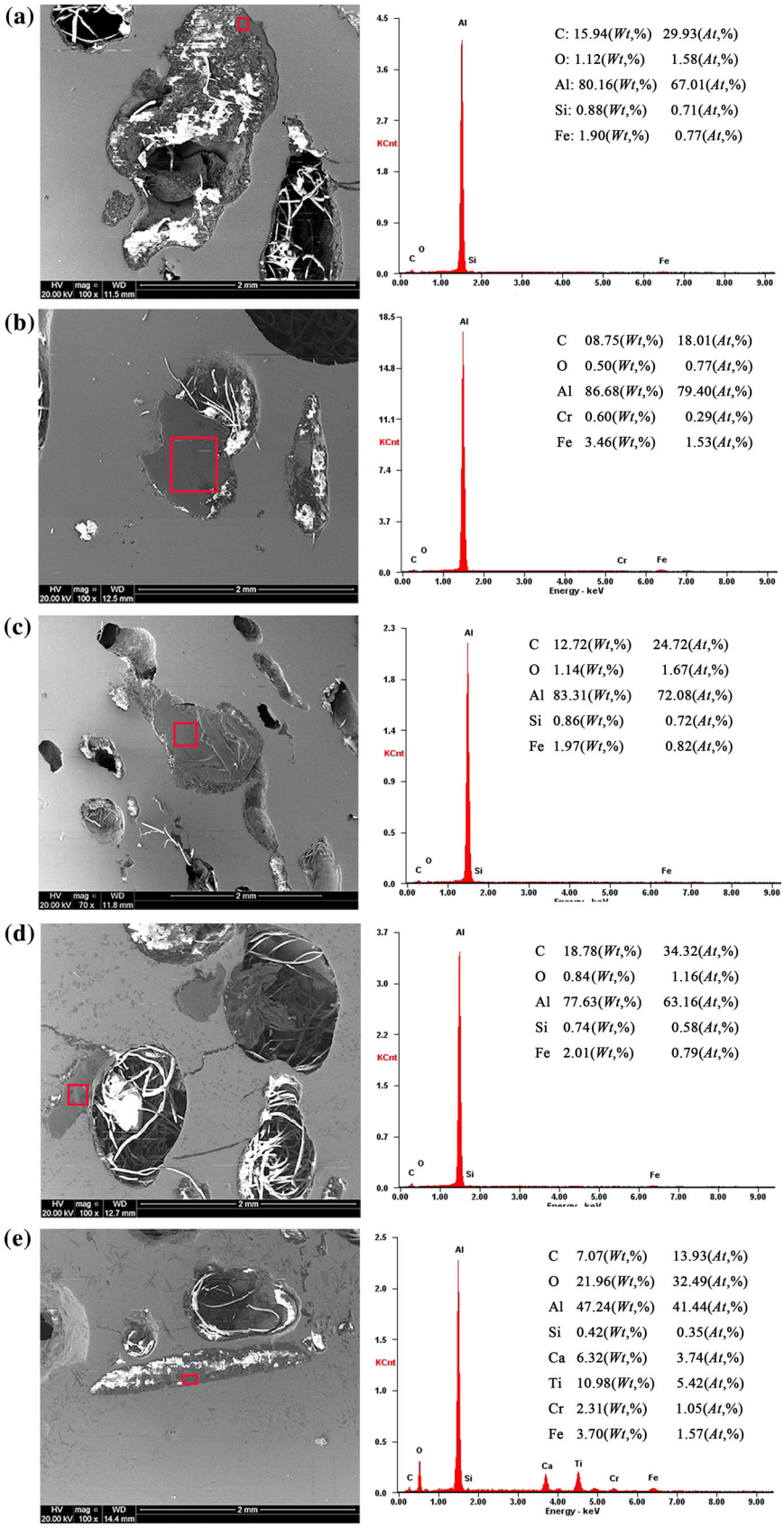

Fig. 7—SEM images and EDS results surrounding the holes in samples with different mass fractions of ceramic particles: (*a*) 5 pct; (*b*) 10 pct; (*c*) 15 pct; (*d*) 20 pct; (*e*) 25 pct.

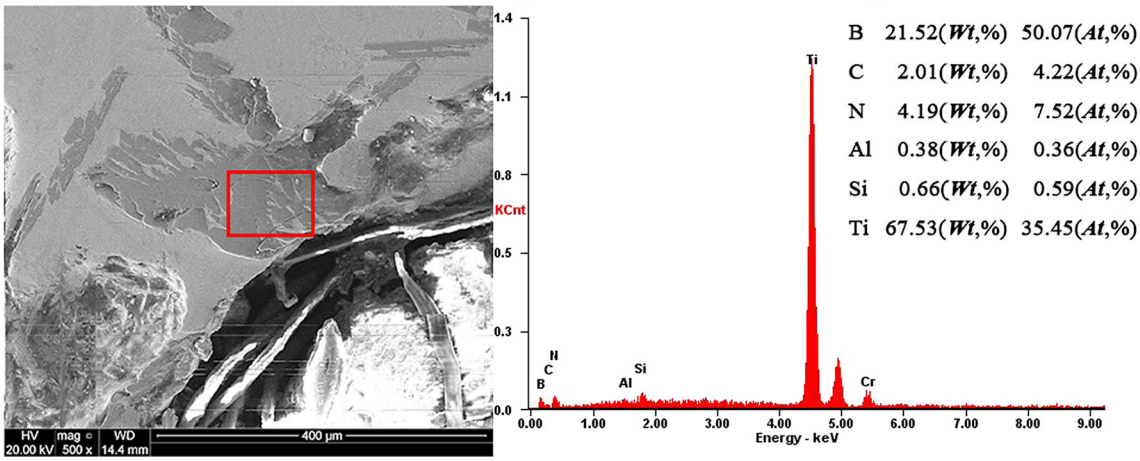

Fig. 8—SEM images and EDS results for samples with ceramic particle contents of 25 pct.

the contact angle between the ceramic particles and the matrix. Accordingly, a composite with a higher ceramic particle content maintains liquid-phase metals for a shorter period, inhibiting the metal flow and backfilling of voids. The bulk of TiB_2 (Figure 8) in the composite with a TiC and TiB_2 content of 25 pct hinders the molten pool flow, spreading, and wetting.

The Cr content in the hole is higher than that in the matrix of samples with ceramic particle contents of 5 to 20 pct (Figures 9(a) through (d)), while it is opposite in samples with ceramic particle contents of 25 pct (Figure 9(e)). This is because the T_{ad} in the experimental systems also exceeds the vapor point of Cr (2945 K). A chromium-rich region will be formed as the chromium gas bubbles remain trapped inside the melt pool during solidification, while a chromium-depleted region will be formed as the surrounding metals with lower Cr contents flow and backfill the voids.

The formation of voids in the composites is related to the vaporization of the reactant Al and the produced Cr, which generates gas bubbles that can remain trapped inside the melt pool during solidification. The temperature and the viscosity of the melt pool decrease with increasing TiC and TiB_2 contents. Thus, the solidification time is shorter, which impacts the metal flow and backfilling of voids. In addition, the number of ceramic particles increases with increasing TiC and TiB_2 contents, which can provide more nuclei for bubble formation. The size of ceramic particles increases with increasing mass fractions, which would have a greater impact on the continuity of the matrix. In addition, the bulk of TiB_2 in the composite has a stronger inhibitory effect on molten pool flow, spreading, and wetting. The inhibitory effect of these factors causes the porosity to increase with increasing ceramic particle content.

Figure 10 shows the average hardness values of the composites (measured twice at the top, middle, and bottom of the products) with ceramic particle different mass fractions. All samples exhibited hardness values exceeding 60 HRC. This can be attributed to the combined effects of grain refinement and grain boundary strengthening. However, the hardness value

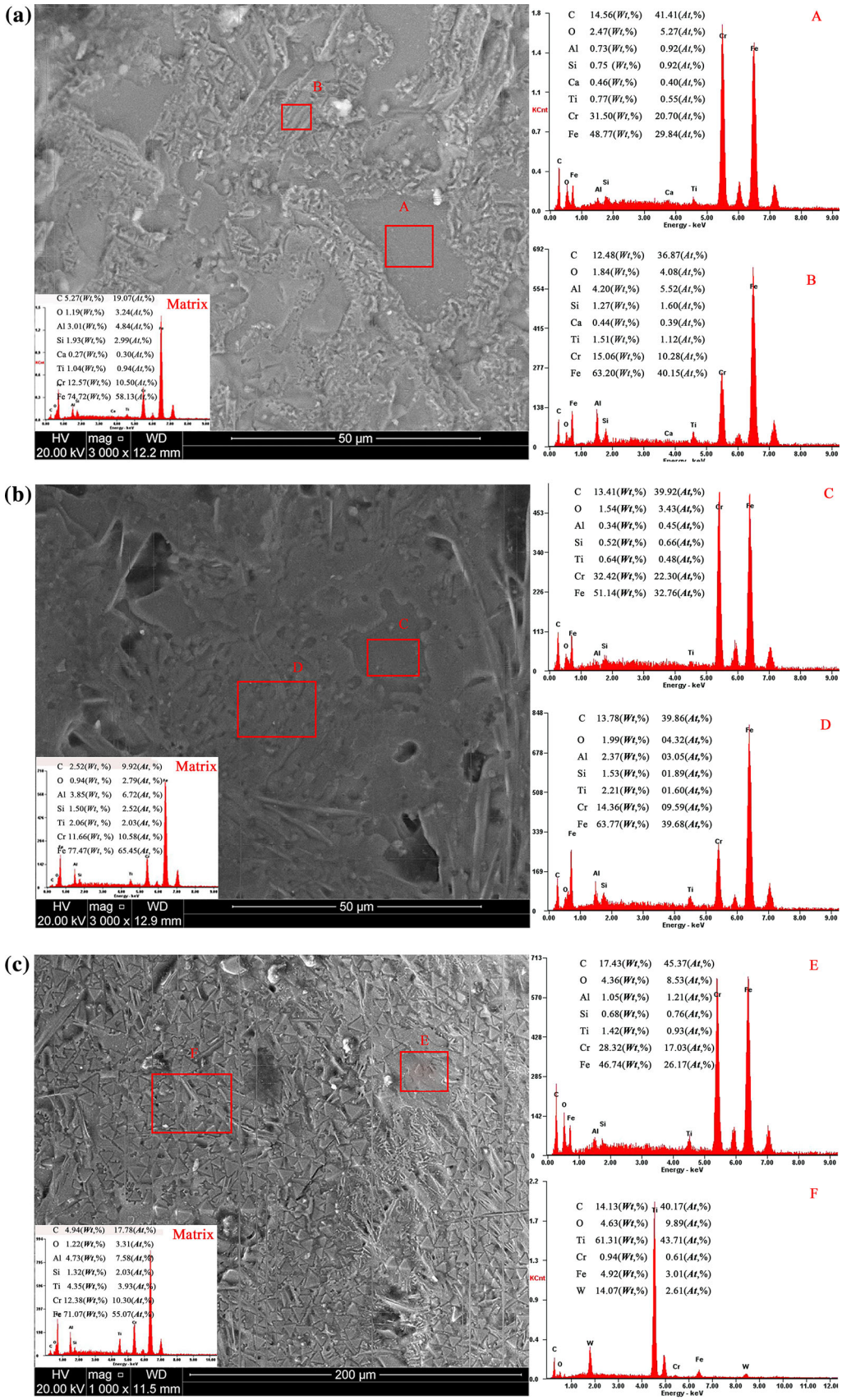

Fig. 9—Compositions surrounding and inside the holes of samples with different ceramic particle mass fractions: (*a*) 5 pct; (*b*) 10 pct; (*c*) 15 pct; (*d*) 20 pct; (*e*) 25 pct.

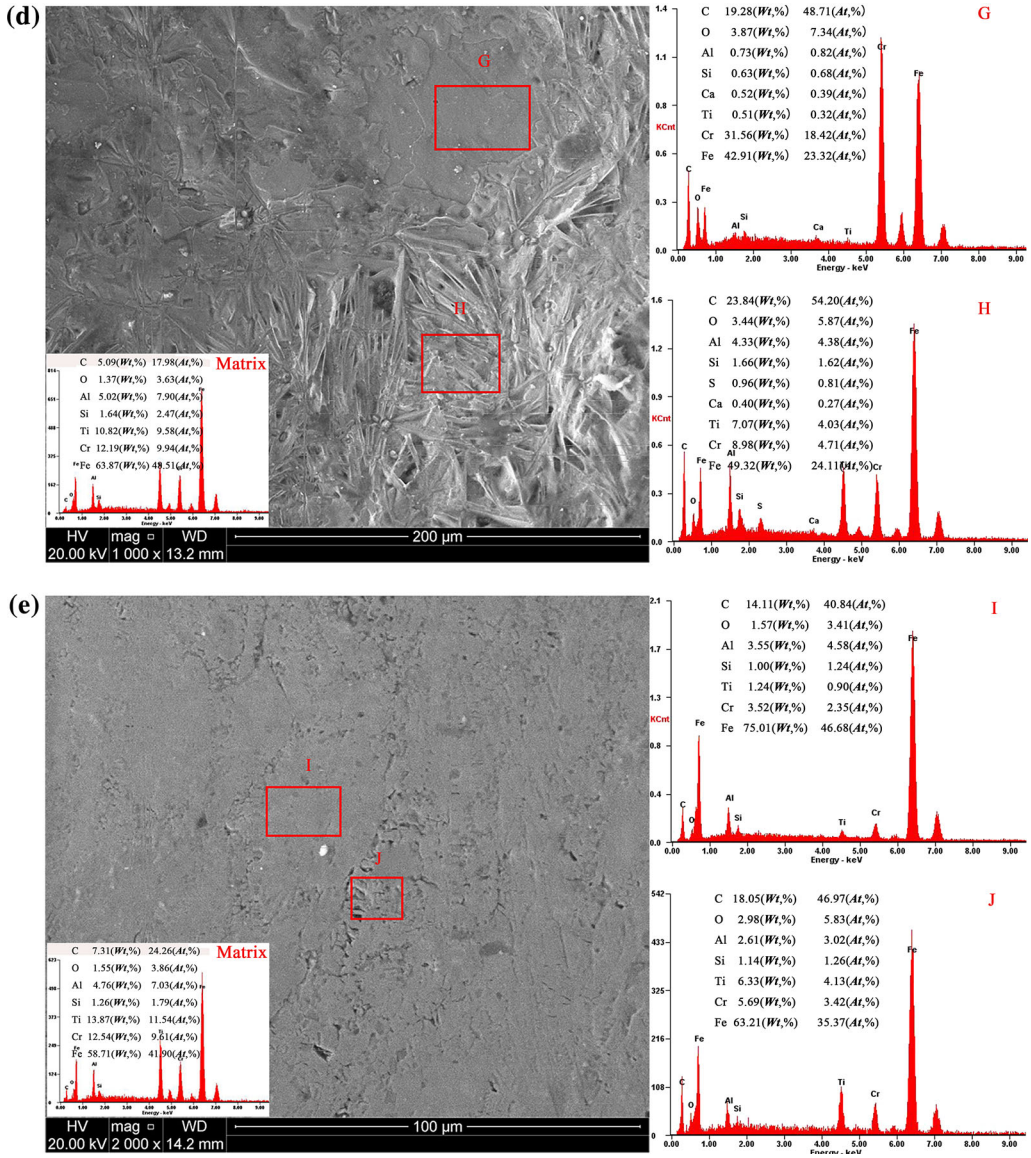

Fig. 9—continued.

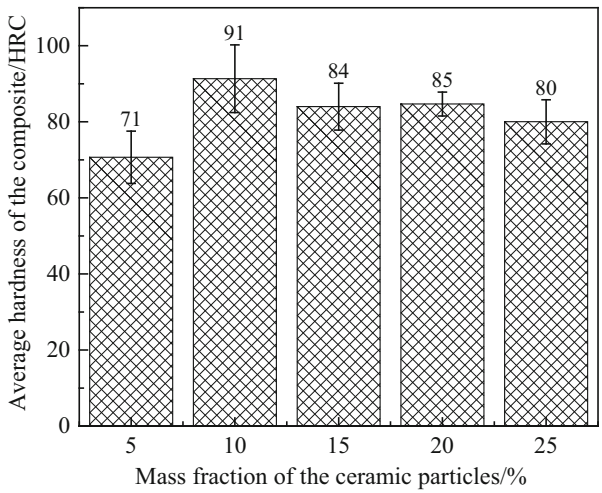

Fig. 10—Influence of ceramic particle mass fraction on the hardness of the composites.

decreases as the mass fractions of ceramic particles increases from 10 to 15 pct, which is directly related to microstructural coarsening that can diminish the pinning effect.

IV. CONCLUSION

Wear-resistant composites are prepared by rapid combustion synthesis from a self-sustained reaction between Ti, Al, CaF_2, B_4C, and CrO_3 powders under a 1.5 MPa Ar atmosphere. The synthesized samples contained holes in the upper surfaces with different ceramic particle contents, where the composite needs to be wearable, which is the product of the reaction. The porosity increases with the mass fraction of the ceramic particles, which may be due to the following reasons:

1. The adiabatic temperatures of the studied system are higher than the vaporization point of the reactant Al and the produced Cr. The vaporization of Al and Cr causes the holes.
2. The inhibition effect of lower temperatures and higher metal viscosities and wetting angles between the liquid and solid phase, higher number of nuclei for bubble formation, and higher destructivity to the continuity of the matrix causes the porosity of the composite to increase with higher contents of TiC and TiB_2.
3. The average hardness values of the composites exceed 60 HRC, which can be attributed to the combined effects of the strengthening of grain refinement and boundaries. However, the hardness value decreases with the coarsening of the ceramic particles.

ACKNOWLEDGMENTS

This work was financially supported by the National Natural Science Foundation of China No. 51471002 and Science and Technology Planning Project of Guangdong Province No. 2016B090931005. One of the authors (Sufen Tao) would like to extend her most sincere gratitude to associate professor Yunjin Xia and professor Jie Li. We are also very grateful to Dr. Zengchao Yang and Jing Zhang for their valuable discussions.

REFERENCES

1. E. Pagounis and V.K. Lindroos: *Mater. Sci. Eng. A*, 1998, vol. 246, pp. 221–34.
2. E. Pagounis, V.K. Lindroos, and M. Talvitie: *Mater. Sci. Eng. A*, 1996, vol. 27, pp. 4171–81.
3. S.C. Tjong and K.C. Lau: *Compos. Sci. Technol.*, 2000, vol. 60, pp. 1141–46.
4. C. Raghunath, M.S. Bhat, and P.K. Rohatgi: *Scripta Metall. Mater.*, 1995, vol. 32, pp. 577–82.
5. Ö.N. Doğan and J.A. Hawk: *Scripta Metall. Mater.*, 1995, vol. 33, pp. 953–58.
6. C.C. Degnan and P.H. Shipway: *Wear*, 2002, vol. 252, pp. 832–41.
7. C.C. Degnan and P.H. Shipway: *Metall. Mater. Trans. A.*, 2002, vol. 33A, pp. 2973–83.
8. I.W.M. Brown and W.R. Owers: *Curr. Appl. Phys.*, 2004, vol. 4, pp. 171–74.
9. B.S. Terry and O.S. Chinyamakobvu: *J. Mater. Sci. Lett.*, 1991, vol. 10, pp. 628–29.
10. Y. Chen: *Scripta Mater.*, 1997, vol. 1997, pp. 989–93.
11. A. Saidi, A. Chrysanthou, J.V. Wood, and J.L.F. Kellie: *J. Mater. Sci.*, 1994, vol. 29, pp. 4993–98.
12. M.J. Capaldi, A. Saidi, and J.V. Wood: *ISIJ Int.*, 1997, vol. 37, pp. 188–93.
13. A. Saidi, A. Chrysanthou, J.V. Wood, and J.L.F. Kellie: *Ceram. Int.*, 1997, vol. 23, pp. 185–89.
14. Q. Fan, H. Chai, and Z. Jin: *J. Mater Sci.*, 1999, vol. 34, pp. 115–22.
15. Q. Fan, H. Chai, and Z. Jin: *J. Mater. Sci.*, 2001, vol. 36, pp. 5559–63.
16. T.K. Bandyopadhyay, S. Chatterjee, and K. Das: *J. Mater Sci.*, 2004, vol. 39, pp. 5735–42.
17. K. Das, T.K. Bandyopadhyay, and S. Das: *J. Mater. Sci.*, 2002, vol. 37, pp. 3881–92.
18. R.J. Li: *Ceramic-metal composites(In Chinese)*, 2nd ed., Metallurgical Industry Press, Beijing, 2004, pp. 242–50.
19. L. Contreras, X. Turrillas, G.B.M. Vaughan, Å. Kvick, and M.A. Rodŕiguez: *Acta Mater.*, 2004, vol. 52, pp. 4783–90.
20. A.G. Merzhanov and I.P. Borovinskaya: *Int. J. Self Propag. High Temp. Synth.*, 2008, vol. 17, pp. 242–65.
21. A. Varma, A.S. Rogachev, A.S. Mukasyan, and S. Hwang: *Adv. Chem. Eng.*, 1998, vol. 24, pp. 179–226.
22. G. Liu, J. Li, and K. Chen: *Int. J. Refract. Met. H.*, 2013, vol. 39, pp. 90–102.
23. D. Ye and J. Hu (Eds): *Handbook of Thermodynamic Data of Inorganic Substances(In Chinese)*, 2nd ed., Metallurgy Industry Press, Beijing, 2002, pp. 842–45.
24. X. Su, F. Fu, Y. Yan, G. Zheng, T. Liang, Q. Zhang, X. Cheng, D. Yang, H. Chi, X. Tang, Q. Zhang, and C. Uhera: *Nat. Commun.*, 2014, vol. 5, pp. 1–7.
25. B. AlMangour, D. Grzesiak, T. Borkar, and J.M. Yang: *Mater. Design*, 2018, vol. 138, pp. 119–28.
26. B. AlMangour, D. Grzesiak, and J.M. Yang: *Powder Technol.*, 2018, vol. 326, pp. 467–78.
27. B. AlMangour, D. Grzesiak, and J.M. Yang: *J Alloy Compd.*, 2017, vol. 706, pp. 409–18.